Vol. 90 (1996) *ACTA PHYSICA POLONICA A* No. 1

Proceedings of the 2nd Winter Workshop S&SRES'96, Polanica Zdrój 1996

SPECTROSCOPIC AND LASER PROPERTIES OF $LiNbO_3:Dy^{3+}$ CRYSTALS

M. MALINOWSKI, P. MYZIAK, R. PIRAMIDOWICZ

Institute of Microelectronics and Optoelectronics PW
Koszykowa 75, 00-662 Warsaw, Poland

I. PRACKA, T. ŁUKASIEWICZ, B. SURMA

Institute of Electronic Materials Technology, Wólczyńska 133, 01-919 Warsaw, Poland

S. KACZMAREK, K. KOPCZYŃSKI AND Z. MIERCZYK

Institute of Optoelectronics WAT, Kaliskiego 2, 01-489 Warsaw, Poland

The spectroscopic properties of trivalent dysprosium (Dy^{3+}) doped $LiNbO_3$ crystals have been investigated at various temperatures. Absorption, emission, excitation and lifetime measurements have been performed and discussed in the framework of Judd–Ofelt approach. The stimulated emission cross sections of the strongest transitions of Dy^{3+} ion have been estimated. A stimulated emission has been demonstrated in the near infrared.

PACS numbers: 71.55.Ht, 78.40.Ha, 78.47.+p, 78.55.Hx

1. Introduction

Rare-earth doped lithium niobate, owing to good electro-optic, acousto-optic and nonlinear properties of the host matrix, offers technologically important possibilities for planar waveguide lasers and amplifiers and received considerable attention in recent years.

Laser action in Nd^{3+}, Ho^{3+} and Tm^{3+} doped $LiNbO_3$ (LNB) has been reported [1] and spectroscopic properties of these crystals as well as Er^{3+} [2] and Cr^{3+} [3] doped materials have been studied. Diode pumped channel waveguide lasers have been realised in Nd^{3+} [4], Yb^{3+} [5] and Er^{3+} [6] activated $LiNbO_3$,

Recent reports indicate the interest of activating the optical glasses by Dy^{3+} ions for the purposes of 1.3 μm band fiber telecommunication [7] and dysprosium is being compared with the most widely used dopant at present — praseodymium [8]. However, literature on the spectroscopy of Dy^{3+} doped materials is not exhaustive and, to our knowledge, laser action in Dy^{3+} activated solids has been only observed at the 3 μm band [9] in BaY_2F_8 crystal.

The aim of this work was to examine a new optically active material which may be of considerable technological significance. We report on the spectroscopic investigation of Dy^{3+} ions in $LiNbO_3$. Various absorption, emission and excitation spectra have been investigated for several activator concentrations at temperatures between 10 and 300 K. Low temperature spectroscopic data were used to establish Dy^{3+} energy level diagram in $LiNbO_3$ and to investigate the inhomogeneous character of optical transitions. The Judd–Ofelt theory has been applied to the optical absorption linestrengths measured at room temperature to determine Ω_i intensity parameters, which were then used to predict the radiative decay rates and branching ratios for transitions from the metastable $^4F_{9/2}$ state of Dy^{3+} ion. These results were compared with those for other known dysprosium systems.

2. Experimental methods

$LiNbO_3:Dy^{3+}$ samples with concentrations 0.31 and 1.7 at.% were grown parallel to the $\langle c \rangle$ direction using the Czochralski technique at I.T.M.E. Laboratory in Warsaw. Fluorescence and excitation spectra were obtained using a tunable laser operating with Coumarine 460-481 dyes, pumped by a nitrogen laser (10 ns pulse length, 10 Hz repetition rate and 10 mJ energy per pulse at 337 nm). CW excitation in the blue region was achieved by a ILA-120 3 W argon ion laser. The spectra were recorded using a GDM-1000 monochromator with dispersion of 11 cm^{-1}/mm and detected by RCA C-31034-02 cooled AsGa photomultiplier. Data acquisition was obtained using a SR 400 photon counting system controlled with a PC computer. Fluorescence lifetime measurements were made using a Tennelec/Nucleus MCS multichannel analyser. Sample cooling was provided by a closed circuit He optical cryostat allowing to vary temperature between 10 and 300 K.

3. Results and discussion

3.1. Absorption and emission spectra

Room temperature absorption spectrum, for the light propagating parallel to the c axis, in the 400–650 nm range of 1.7% Dy^{3+} doped $LiNbO_3$ is presented in Fig. 1. It shows several, characteristic for the $4f^9 \rightarrow 4f^9$ transitions of trivalent dysprosium, groups of lines which correspond to transitions from the $^6H_{15/2}$

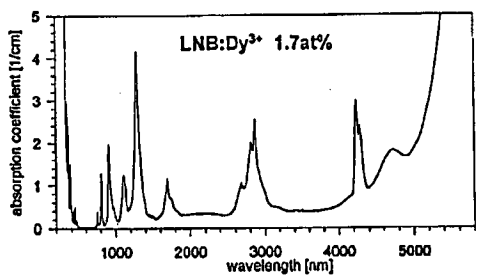

Fig. 1. Absorption spectrum of 1.7 at.% $Dy^{3+}:LiNbO_3$ crystal at room temperature.

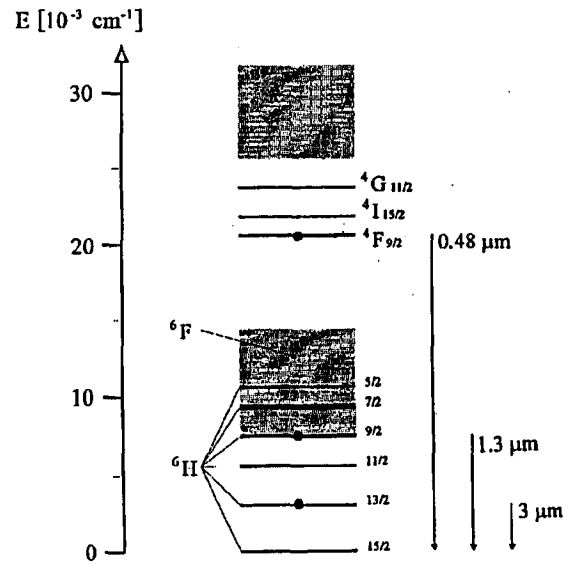

Fig. 2. Energy level scheme of an isolated Dy^{3+} ion. Emission transitions reported in literature are indicated by arrows [1, 7, 8, 16].

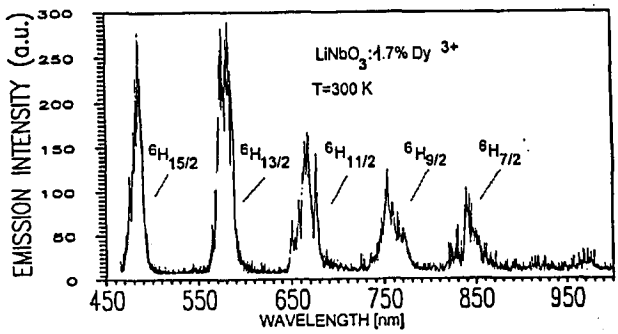

Fig. 3. Room temperature visible emission spectrum of Dy^{3+} in $LiNbO_3$ crystal.

ground state to the different multiplets, see also energy level scheme in Fig. 2. Below about 500 nm the background absorption of the host crystal begins to increase and it grows rapidly at about 250 nm. After excitation by the 476 nm blue line of an argon laser, emission of the crystals was recorded between 300 nm and 2 μm. Figure 3 illustrates the room temperature emission spectrum of 1.7% Dy^{3+} : $LiNbO_3$ in the visible range, no infrared (IR) emission was detected. It was concluded that in $LiNbO_3 : Dy^{3+}$ visible fluorescence is due to transitions from the excited $^4F_{9/2}$ state to the lower $^6H, F_J$ states and, though these transitions are forbidden by the spin selection rule, they were observed as relatively intense.

It could be seen that room temperature lines are too broad for precise as-

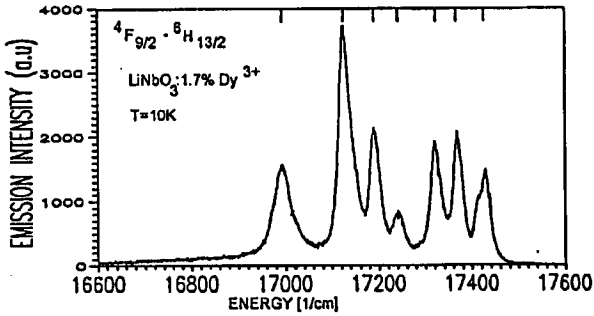

Fig. 4. Part of the visible emission spectrum of Dy^{3+} in $LiNbO_3$ crystal measured at 10 K.

TABLE I

Energy levels of Dy^{3+} ion in $LiNbO_3$ measured at 10 K.

$[SLJ]$ manifold	E [cm^{-1}]
$^6H_{15/2}$	0, 14, 45, 113, 222, 303, 422, 603
$^6H_{13/2}$	3535, 3595, 3643, 3725, 3775, 3840, 3969
$^6H_{11/2}$	5878, 5928, 5991, 6059, 6117, 6221
$^6H_{9/2}+{}^6F_{11/2}$	7678, 7700, 7749, 7798*, 7815, 7843, 7891, 7937, 8004, 8093*
$^6H_{7/2}+{}^6F_{9/2}$	90621, 91655, 92060, 93526, 9838, 9853, 9878, 9943, 9979, 10035
$^6H_{5/2}$	–
$^6F_{7/2}$	11080, 11108, 11143*, 11176*
$^6F_{5/2}$	12445, 12487, 12555
$^6F_{3/2}$	13271, 13318*
$^6F_{1/2}$	–
$^4F_{9/2}$	20963, 20974*, 21069, 21097, 21113
$^4I_{15/2}$	21945, 21953, 21978, 22009, 22211, 22216, 22255

* denotes less accurate results.

signment. The determination of individual Stark levels of the Dy^{3+} ions was made by analysing various low temperature absorption, excitation and dye laser excited emission spectra which showed sharper lines, see Fig. 4. The linewidth of the lowest Stark component of the $^4F_{9/2}$ metastable state in 0.3% Dy^{3+} crystal was measured to be 4 cm^{-1} at 10 K, indicating a smaller amount of the inhomogeneous broadening than reported for Er^{3+} ion in $LiNbO_3$ [10]. A summary of the energy levels derived from our measurements is given in Table I.

3.2. Optical transition intensity analysis

Once the energy levels have been determined, the Judd–Ofelt [11, 12] intensity analysis was performed using the π and σ polarised absorption spectra as

proposed in Ref. [13]. Since the details of the Judd–Ofelt theory, its precision and drawbacks have been extensively analysed elsewhere [11–13] we have presented here only the essential results. The central result of the Judd–Ofelt theory is that the oscillator strength f_{calc} of an electric dipole transition between rare-earth ion multiplets ($J \rightarrow J'$) can be expressed by

TABLE II

Measured and calculated oscillator strengths for Dy^{3+} ion in $LiNbO_3$.

$[S'L'J']$ manifold	λ [nm]	f_{exp} $[10^{-6}]$	f_{calc}
$^6H_{13/2}$	2869	3.94	2.48
$^6H_{11/2}$	1690	2.25	2.12
$^6H_{9/2}+{}^6F_{11/2}$	1290	13.06	13.12
$^6H_{7/2}+{}^6F_{9/2}$	1100	2.49	4.34
$^6F_{7/2}$	910	3.28	3.37
$^6F_{5/2}$	806	1.56	1.52
$^6F_{3/2}$	757	0.290	0.287
$^4F_{9/2}$	475	0.241	0.265
$^4I_{15/2}$	453	0.830	0.773
$^4G_{11/2}$	428	0.417	0.15
$^4F_{7/2}+{}^4I_{13/2}+{}^4M_{21/2}$	390	3.96	3.78
$^4M_{19/2}+{}^4P_{5/2}$	372	3.70	2.48
$^4I_{11/2}+{}^4P_{7/2}$	358	6.71	6.26

RMS dev. $= 2.24 \times 10^{-7}$, $\Omega_2 = 9.57 \times 10^{-20}$ cm^2, $\Omega_4 = 2.63 \times 10^{-20}$ cm^2, $\Omega_6 = 2.52 \times 10^{-20}$ cm^2.

$$f_{\text{calc}}(aJ, bJ') = \frac{8\pi^2 m\nu}{3h(2J+1)n^2}\chi \sum_{t=2,4,6} \Omega_t \left|\langle 4f^n|a, J||U^{(t)}||4f^n|b, J'|\rangle\right|^2, \quad (1)$$

where h is Planck's constant, J is the angular momentum of the initial level, $\chi = n(n^2+2)^{2/9}$ is a local field correction factor, $\langle a \parallel U^{(t)} \parallel b\rangle$ are the doubly reduced matrix elements and Ω_t are empirically determined parameters. The experimental oscillator strength f_{exp} for an absorption transition is defined as

$$f_{\text{exp}} = \frac{mc^2}{\pi e^2}\int \sigma(\nu)\mathrm{d}\nu, \quad (2)$$

where m and e are the electron mass and charge, respectively, c is the light velocity, ν is the optical frequency and $\sigma(\nu)$ is the absorption cross section.

From the least square fit of measured f_{exp} and calculated f_{calc} oscillator strengths the three intensity Ω_t parameters were evaluated. In performing the calculations the reduced matrix elements were taken from Carnall et al. [14] and the index of refraction n as a function of wavelength was taken from Ref. [15]. Table II shows the average wavelengths for the analysed transitions together with

TABLE III

Predicted radiative transition probabilities A and branching ratios β from the $^4F_{9/2}$ level of Dy^{3+} ion in $LiNbO_3$. $\tau_R = 298$ μs.

Final state $[S'L'J']$	λ [nm]	A [s^{-1}]	β_{calc} [%]	β_{meas} [%]
$^6H_{15/2}$	475	557	17	20
$^6H_{13/2}$	569	2337	69	46
$^6H_{11/2}$	661	228	7	17
$^6H_{9/2}+^6F_{11/2}$	752	118	3.7	9
$^6H_{7/2}+^6F_{9/2}$	836	72	2	8
$^6H_{5/2}+^6F_{7/2}$	1014	19	0.6	0
$^6F_{5/2}$	1180	24	0.7	0
$^6F_{3/2}$	1305	0	0	0

the measured f_{exp} and calculated f_{calc} oscillator strengths for all measured absorption transitions. The resulting set of Judd–Ofelt parameters was found to be $\Omega_2 = 9.57 \times 10^{-20}$ cm^2, $\Omega_4 = 2.63 \times 10^{-20}$ cm^2 and $\Omega_6 = 2.52 \times 10^{-20}$ cm^2. The fit between the measured and calculated oscillator strengths values, shown in Table II, was good as indicated by the root mean square (RMS) deviation of 2.24×10^{-7} which is comparable to values found by applying Judd–Ofelt theory to Dy^{3+} ion in other systems [7, 16]. It could be noticed that LNB presents oscillator strengths for the absorption transitions very similar to those of oxide glasses [16]. From the calculated set of Ω_t intensity parameters the electric dipole transition probabilities $A(aJ, bJ')$ for emission between J manifolds of Dy^{3+} were calculated using the following equation:

$$A(aJ, bJ') = \frac{64\pi^4 e^2 \nu^3}{3h(2J+1)c^3} \chi \sum_{t=2,4,6} \Omega_t \left| \langle 4f^n | a, J || U^{(t)} || \langle 4f^n | b, J' | \rangle \right|^2 . \qquad (3)$$

Calculated radiative transition probabilities A from the excited $^4F_{9/2}$ state together with the resulting branching ratios β_{calc} are given in Table III. Six emission bands were observed due to the transitions from the $^4F_{9/2}$ level to lower excited states, see Fig. 3. The corresponding branching ratios were obtained from the nonpolarised fluorescence spectra by comparing relative areas under the emission peaks and are listed in the last column of Table III. It could be seen that the highest calculated value of the branching ratio is for the $^4F_{9/2} \rightarrow {}^6H_{13/2}$ transition which is found to be in agreement with the experimentally determined β_{meas} value. The largest discrepancy between experiment and theory is for the $^4F_{9/2} \rightarrow {}^6H_{15/2}$ transition, where the measured branching ratio is substantially longer than the calculated value. The radiative lifetime of the $^4F_{9/2}$ state was calculated to be 298 μs and compares reasonably with the radiative lifetime value of 371 μs found for oxide glass [16]. However, radiative lifetime calculated for the fluorozincate glass was much longer, of 1.26 ms [17].

3.3. Fluorescence dynamics and time-resolved experiments

Figure 5 shows the decay profiles of the $^4F_{9/2}$ level. For all investigated Dy^{3+} concentrations these decays are slightly nonexponential suggesting that the concentration quenching could be active for concentration as low as 0.3% of dysprosium. From the long time part of the decay the fluorescence lifetime was determined to be of 245 μs. The time behaviour of the $^4F_{9/2}$ fluorescence in $LiNbO_3$ was studied at different temperatures and was found to be nearly temperature and activator concentration independent between 10 and 300 K suggesting its predominantly radiative character. This is consistent with the large energy gap of 7680 cm^{-1} to the next lower lying level. Difference between calculated radiative and experimental lifetimes of Dy^{3+} could be due to the overestimation of the actual concentration of activator in the investigated sample. It is also possible that the $^4F_{9/2}$ emission is affected by the background absorption of the $LiNbO_3$ host.

Time-resolved (TR) excitation spectroscopy has been used for further studies of the character of line broadening. The dye laser was scanned across the $^6H_{15/2}$ (1) $\rightarrow$ $^4F_{9/2}$ absorption and the total $^4F_{9/2}$ fluorescence was registered at various delays after the excitation pulse. From comparison of the excitation spectra presented in Fig. 6 no linewidth or lineshape variation with the delay time could be observed which suggests the same Pr^{3+} ions in $SrLaGa_3O_7$ lattice; longer lived regular ions and ions in minority sites characterised by much stronger coupling to the lattice and efficient nonradiative decay.

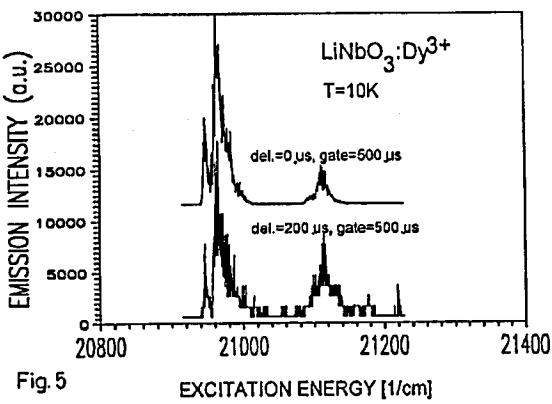

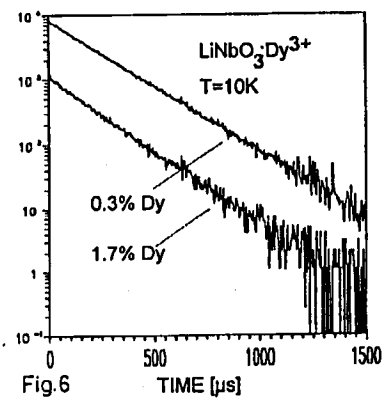

Fig. 5. Fluorescence decays at 10 K in $LiNbO_3$ crystals with 0.3 and 1.7 at.% of Dy^{3+}.
Fig. 6. Time-resolved excitation spectra of the $^6H_{15/2} \rightarrow {}^4F_{9/2}$ transition in Dy^{3+}: $LiNbO_3$ at 10 K.

When comparing various dysprosium doped media [12, 13, 16] it is apparent that the emission properties of $LiNbO_3$ are more influenced by nonradiative processes.

By comparing the polarised resonant absorption and emission spectra the emission cross section σ_{em} of the visible emissions has been determined. The strongest fluorescence peaks at 485 nm and 580 nm are characterised by

$\sigma_{em}(485\ nm) = 1.6 \times 10^{-21}\ cm^2$ and $\sigma_{em}(580\ nm) = 7.8 \times 10^{-21}\ cm^2$ value. The emission cross section could be also calculated from the absolute transition probability and the fluorescence linewidth

$$\sigma_{em} = \frac{\lambda^2 \beta}{8\pi c n^2 \tau_R \Delta\nu_{eff}}, \tag{4}$$

where λ is the wavelength of the fluorescence peak, $\Delta\nu_{eff}$ is the effective fluorescence linewidth and β and τ_R are branching ratio and radiative lifetime, respectively. Using the measured values (see Fig. 1 and Table I) and the results of Judd–Ofelt calculations (see Table III) the emission cross sections were found to be $\sigma_{em} = 2.2 \times 10^{-21}\ cm^2$ and $\sigma_{em} = 12 \times 10^{-21}\ cm^2$, respectively for 485 nm and 580 nm transitions. It is seen that the blue emission cross section value calculated from the emission spectra is lower than the theoretical one which may be due to reabsorption and excited state absorption losses.

The spectroscopic properties of various Dy^{3+} doped materials, which are relevant to the visible laser operation, are compared in Table IV. Till now we have only observed a stimulated emission in the 790 nm band.

TABLE IV

Comparison of the spectroscopic properties of Dy^{3+} doped materials.

Host	Ω_2 [10^{-20} cm^2]	Ω_4 [10^{-20} cm^2]	Ω_6 [10^{-20} cm^2]	Refs.
$LiNbO_3$	9.57	2.63	2.52	this work
LaF_3	1.1	1.4	0.9	[14]
ZnO–TeO_2 glass	4.28	1.32	2.53	[16]
ZnF_2–CdF_2 glass	1.38	1.05	2.35	[17]
ZBLAN	2.7	1.8	2.0	[18]

Host	$^4F_{9/2}$ rad. τ_0 [μs]	$^4F_{9/2}$ fluor. τ_{fl}[μs]	$^4F_{9/2}$–$^6H_{13/2}$ β_{meas}	$^4F_{9/2}$–$^6H_{15/2}$ β_{meas}
$LiNbO_3$	298	245	0.20	0.46
ZnO–TeO_2 glass	371	375	0.30	0.61
ZnF_2–CdF_2 glass	2100	1260	0.27	0.5

4. Conclusions

The spectroscopic properties of Dy^{3+} ion in $LiNbO_3$ crystals were studied and analysed. Polarised absorption spectra have been obtained leading to the determination of the energy level diagram and Judd–Ofelt intensity parameters. Because of the high effective phonon energy of the host matrix of 880 cm^{-1}, dysprosium ion fluorescence in LNB is strongly affected by nonradiative decay, resulting in the absence of the $^6H_{9/2}$ infrared emission. Visible Dy^{3+} fluorescence presents similar lifetime to this of dysprosium doped oxide glasses, these observations are

supported by the theoretical calculations. Spectra registered at cryogenic temperatures indicated lower, than reported for other doped $LiNbO_3$ crystals, degree of the inhomogeneous line broadening and no multisite structure of lines was observed. Emission cross sections, which are relevant to the operation of a visible laser, have been determined and the pulsed infrared light generation at 750.5 nm has been observed for the first time in the plane parallel resonator. It is expected that optimization of the Dy^{3+} ion concentration, resonator configuration and the crystal length will lead to low threshold operation at several other visible emission channels.

References

[1] L.F. Johnson, A.A. Ballman, *J. Appl. Phys.* **40**, 297 (1969).

[2] G. Dominiak-Dzik, S. Gołąb, I. Pracka, W. Ryba-Romanowski, *Appl. Phys. A* **58**, 551 (1994).

[3] J. Garcia Sole, A. Monteil, G. Boulon, E. Camarillo, J.O. Tocho, I. Vergara, F. Jaque, *J. Phys. (France) IV* 1, 403 (1991).

[4] S.J. Field, D.C. Hanna, D.P. Scheperd, A.C. Tropper, *Opt. Lett.* **16**, 481 (1991).

[5] J.K. Jones, J.P. De Sandro, M. Hempstead, D.P. Sheppard, A.C. Large, A.C. Tropper, J.S. Wilknson, *Rare Earth Doped Optical Waveguides, Les Houches, 22 June 1994*, Ed. B. Jacquier, University of Lyon, 1994, p. 827.

[6] J. Sochtig, R. Groß, I. Bauman, W. Sohler, H. Schutz, R. Widmer, *Electron. Lett.* **31**, 551 (1995).

[7] B.N. Samson, J.A. Medeiros Neto, R.I. Laming, D.W. Hewak, *Electron. Lett.* **30**, 968 (1994).

[8] B.N. Samson, J.A. Medeiros Neto, R.I. Laming, D.W. Hewak, *Electron. Lett.* **30**, 1617 (1994).

[9] L.F. Johnson, H.J. Guggenheim, *Appl. Phys. Lett.* **23**, 96 (1973).

[10] D.M. Gill, J.C. Wright, L. McCaughan, *Appl. Lett.* **64**, 2483 (1994).

[11] B.R. Judd, *Phys. Rev.* **127**, 750 (1962).

[12] G.S. Ofelt, *J. Chem. Phys.* **37**, 511 (1962).

[13] A.A. Kaminskii, *Laser Crystals*, 2nd ed., Springer, Berlin 1990.

[14] W.T. Carnall, H. Crosswhite, H.M. Crosswhite, *Energy Level Structure and Transition Probabilities of the Trivalent Lanthanides in LaF_3*, Argonne National Laboratory, Argonne (Illinois) 1975.

[15] C.A. Morrison, R.P. Leavit, in: *Handbook on the Physics and Chemistry of Rare-Earth*, Eds. K.A. Gschneidner, L. Eyring, North-Holland Publ.Co., New York 1982, p. 461.

[16] J. Hormadaly, R. Reisfeld, *J. Non-Cryst. Solids* **30**, 337 (1979).

[17] R. Cases, M.A. Chamarro, R. Alcala, V.D. Rodriguez, *J. Lumin.* **48-49**, 509 (1991).

[18] V.M. Orera, P.J. Alonso, R. Cases, R. Alcala, *Phys. Chem. Glasses* **29**, 59 (1988).